Electrochemical Behaviour and Electrorefining of Cobalt in NaCl-KCl-K_2TiF_6 Melt

Sergey A. Kuznetsov, Olga S. Kazakova, and Olga V. Makarova

Institute of Chemistry, Kola Science Centre RAS, 14 Fersman Str., 184209 Apatity, Murmansk region, Russia

Reprint requests to Prof. S.A. K.; Fax: +7 815 55 61658, E-mail: kuznet@chemy.kolasc.net.ru

Z. Naturforsch. **64a,** 485 – 491 (2009); received June 16, 2008 / revised November 10, 2008

The electrorefining of cobalt in NaCl-KCl-K_2TiF_6 (20 wt%) melt has been investigated. It was shown that complexes of Ti(III) and Co(II) appeared in the melt due to the reaction 2Ti(IV) + Co → 2Ti(III) + Co(II) and this reaction was entirely shifted to the right hand side. On the base of linear sweep voltammetry diagnostic criteria it was found that the discharge of Co(II) to Co metal is controlled by diffusion. The limiting current density of discharge Co(II) to metal in NaCl-KCl-K_2TiF_6 (20 wt%) melt was determined by steady-state voltammetry. The electrorefining of cobalt was carried out in hermetic electrolyser under argon atmosphere. Initial cathodic current density was changed from 0.2 A cm^{-2} up to 0.7 A cm^{-2}, the electrolysis temperature varied within 973 – 1123 K. Behaviour of impurities during cobalt electrorefining was discussed. It was shown that electrorefining led to the elimination of most of the interstitial impurities (H_2, N_2, O_2, C), with the result that the remaining impurity levels below 10 ppm impart high ductility to cobalt.

Key words: Cobalt; Molten Salts; Electrochemical Studies; Electrorefining; High Ductility.

1. Introduction

High-purity cobalt with low metal impurity content can be produced by electrorefining in aqueous solution. However, the content of interstitial impurities H_2, N_2, O_2, C, (hydrogen and oxygen impurities in particular), also remains fairly high after electrorefining. At the same time, ductile alloy production needs cobalt that is free from not only metal impurities, but also interstitial impurities since it is the latter that impart brittleness to the metal at low temperatures. The task of obtaining high purity, cobalt free from interstitial impurities can be solved by using aprotonic solvents, among which are molten salts. In the case of small scale production of high-purity cobalt, it is worthwhile employing electrolytic refining in melts since the resulting cobalt is pliant and the electrorefining process is intensified by at least an order of magnitude compared with aqueous electrolytes.

To our best knowledge no studies on cobalt electrorefining in molten salts have been previously reported. The aim of this research is the study of cobalt and impurities behaviour during cobalt electrorefining in NaCl-KCl-K_2TiF_6 (20 wt%) melt to produce ductile cobalt with minimum interstitial impurity content. It should be noted that electrolytes containing K_2TiF_6 allows the production of cobalt salts in situ, as will be shown below.

2. Experimental

2.1. Chemicals

Alkali chlorides (NaCl and KCl) were purchased from Prolabo (99.5% min.). They were dehydrated by continuous and progressive heating just above the melting point under gaseous HCl atmosphere in quartz ampoules and then fused under high purity argon (U-grade: $<$ 3 ppm H_2O and $<$ 2 ppm O_2). After that molten salts were dehydrated by bubbling HCl gas through the melt during 30 – 50 min. Excess HCl was removed from the melt by argon.

Sodium and potassium chlorides were mixed in the required ratio, placed in a glassy carbon ampoule (SU-2000 type) or molybdenum crucible and transferred to a sealed stainless steel retort. The latter was evacuated to a residual pressure of 0.67 Pa, first at room temperature and then stepwise at 473 K, 673 K and 873 K. The cell was heated using a programmable furnace and temperatures were measured using a Pt-Rh (10 wt%)-Pt thermocouple. The retort was then filled with high purity argon and the electrolyte was melted.

The potassium hexafluorotitanate used in this experiment was obtained by recrystallization of K_2TiF_6 "pure" brand from anhydrous hydrofluoric acid. After washing with ethanol and drying under vacuum, the precipitate was identified by X-ray powder diffraction (XRD), IR spectroscopy, and optical crystallography analyses. Analysis of cobalt before and after electrorefining, and K_2TiF_6 was performed by spectrographic semiquantitative examination. The main impurities in K_2TiF_6 after recrystallization were (ppm): Si (100); Fe (100); Al (30); Mg (3). The concentration of titanium and cobalt in molten salts was determined by a Plasma 400 inductively coupled plasma atomic emission spectrometer (ICP-AES).

2.2. Electrochemical Studies

Linear sweep voltammetry (LSV) and cyclic voltammetry (CV) were employed, using a VoltaLab-40 potentiostat with the software "VoltaMaster 4", version 6. The potential scan rate (v) was varied between $5 \cdot 10^{-3}$ V s^{-1} and 5.0 V s^{-1}. Experiments were carried out in the temperature range 973 – 1123 K. The voltammetric curves were recorded on a glassy-carbon and platinum electrode (diameter of 2 mm and 1 mm, respectively) relative to a quasi-reference electrode from glassy-carbon, of SU-2000 brand. A glassy-carbon SU-2000 crucible served both as container for the melt and auxiliary electrode. While the potential of this quasi-reference electrode does not constitute a thermodynamic reference, the use of this electrode was preferred in order to avoid any contact between the melt and oxygen-containing material as used in classical reference electrodes.

Electrorefining was performed in the electrolyser shown in Figure 1. It consists of four main parts: a retort (5), a transitional chamber (4), a lid (9), and a furnace with resistive heating (6). The electrolyte (11) and metal to be refined, in a plate-holder provided with a diaphragm (12), were loaded into the crucible (13). Temperatures were obtained using thermocouple (7). The cathode (3), on the current lead (1), after conducting a known amount of electricity was slowly lifted from the electrolyte to the lock-chamber (2) to cool. The hermetic damper (10) overlapped the space between the lock-chamber and the retort to preserve the inert atmosphere over the melt.

The cooling of the retort flange, transitional chamber, and lid was performed in water to eliminate the destruction of the vacuum padding and speed up the cathode cooling. After changing the cathode the lock-chamber was evacuated and filled with inert gas and the damper (10) was opened to immerse the cathode in the melt. The luting nut (8) served for fixing the cathode position and sealing of the electrolyser.

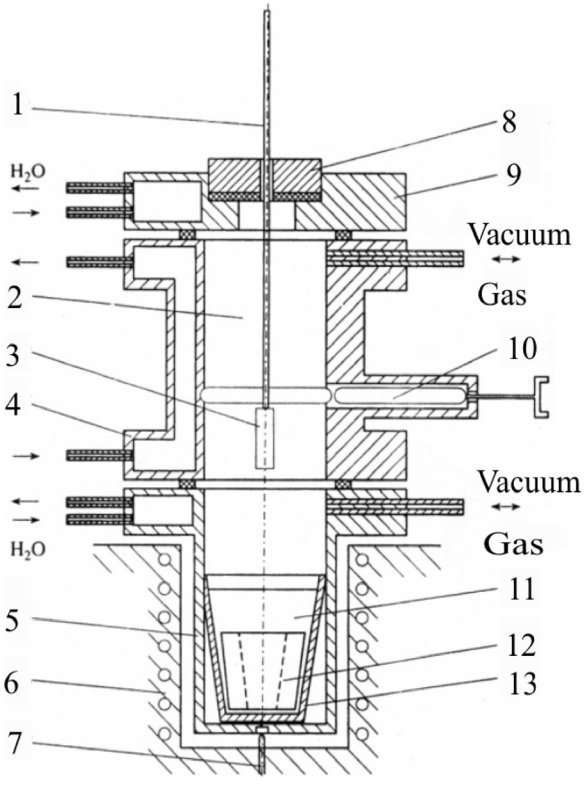

Fig. 1. Scheme of electrolyser for cobalt electrorefining in molten salts. Description in the text.

An equimolar mixture of NaCl-KCl containing 20 wt% K_2TiF_6 was used as the electrolyte. The initial cathodic current density was 0.2 – 0.7 A cm^{-2} and the electrolysis temperature was varied between 973 – 1123 K.

3. Results and Discussion

3.1. Electrochemical Studies

Figure 2 shows a typical voltammetric curve for the NaCl-KCl melt using a glassy-carbon electrode. Along with the cathodic process of alkali metal reduction (R_{Na}^+, R_K^+) there is a peak showing the electrochemical insertion of alkali metals into carbon with the formation of intercalation compounds $R_{int.}$ [1]. The process of intercalation compounds formation has been

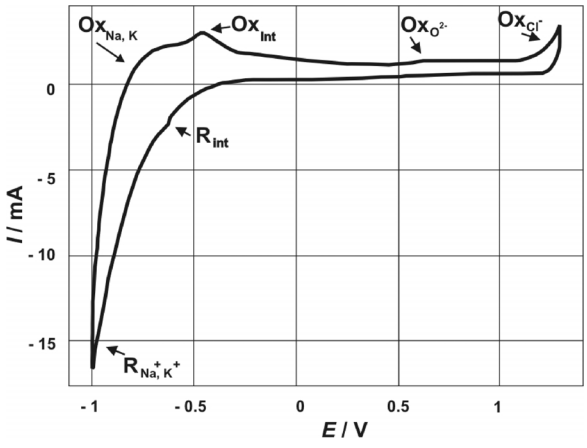

Fig. 2. Cyclic voltammogram at the glassy carbon electrode in an equimolar NaCl-KCl melt. Area: 0.296 cm^2; sweep rate: 1.0 $V\,s^{-1}$; temperature: 1023 K; quasi-reference electrode: glassy-carbon.

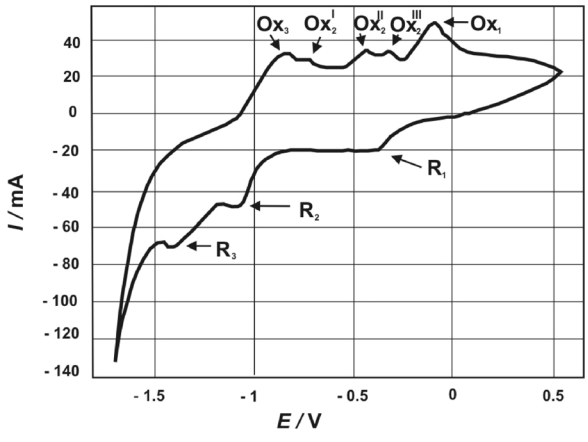

Fig. 3. Cyclic voltammetric curve at a platinum electrode in NaCl-KCl-K_2TiF_6 melt. Area: 0.322 cm^2; sweep rate: 1.0 $V\,s^{-1}$; temperature: 1023 K; concentration of $K_2TiF_6 = 3.2 \cdot 10^{-4}$ $mol\,cm^{-3}$; quasi-reference electrode: glassy-carbon.

thoroughly examined [2]. In the anodic semi cycle, the volammogram reveals four peaks: alkali metals (Ox_{Na}, Ox_K) and intercalation compounds ($Ox_{int.}$) dissolution, electrooxidation of oxygen anions (with CO and CO_2 formation ($Ox_O{}^{2-}$) [3] and chlorine anions ($Ox_{Cl}{}^{-}$ with Cl_2 formion). The small $Ox_O{}^{2-}$ wave suggests that the content of oxygen anions in the NaCl-KCl melt after the procedures described above in 2.1 is relatively small.

The cyclic voltammogram obtained at a platinum electrode after K_2TiF_6 addition to the equimolar NaCl-KCl melt is given in Figure 3. The electroreduction process of the $[TiF_6]^{2-}$ complex in NaCl-KCl melt, including at a platinum electrode, has been reported in detail [4]. Our voltammetric curve has the same shape as that in [4]. We therefore attribute peak R_1 to the electroreduction $Ti(IV) + e^- \rightarrow Ti(III)$, and peak Ox_1 to Ti(III) oxidation to Ti(IV).

The cathodic peak R_2 and anodic peaks of dissolution Ox_2^I, Ox_2^{II}, Ox_2^{III} correspond to the formation and subsequent dissolution of intermetallic compounds of platinum with titanium (Fig. 3). That the process of intermetallic compounds formation in the region of wave R_2 potentials did take place was confirmed by potentiostatic electrolysis. Thus, at the foot of wave R_2 the compound $TiPt_3$ was obtained. At this polarization rate, the process of titanium and platinum alloy formation is characterized by one cathodic wave R_2, although lower rates ($v \leq 0.5$ $V\,s^{-1}$) reveal at least two cathodic waves corresponding to intermetallic compound formation between platinum and titanium. At the same time, the only cathodic wave R_2 in the anodic semi cycle corresponds to three waves of the dissolution of three intermetallic compounds, which agrees with the Pt-Ti equilibrium diagram containing the compounds Ti_3Pt, TiPt, $TiPt_3$ [5, 6]. Since the dissolution potentials of titanium-enriched alloys have more negative dissolution potentials, the Ox_2^I, Ox_2^{II}, Ox_2^{III} waves can be attributed to Ti_3Pt, TiPt and $TiPt_3$ dissolution, respectively. Peak R_3 corresponds to the electroreduction $Ti(III) + 3e^- \rightarrow Ti$ [4] on the surface of intermetallic compounds and peak Ox_3 is connected with titanium dissolution.

Figure 4 shows the voltammetric curve of NaCl-KCl-K_2TiF_6 melt in contact with cobalt. It is clear that the voltammogram contains, along with the waves inherent to K_2TiF_6 (R_1, Ox_1 and R_3, Ox_3), two new waves (R_4, Ox_4 and R_5, Ox_5) in comparison with the polarization curve (Fig. 3). When cobalt metal is added to the melt, wave R_1 becomes cathodic-anodic (Fig. 4), which suggests the appearance in the melt of Ti(III) complexes as the result of Ti(IV) interaction with cobalt metal according to

$$2\,Ti(IV) + Co \leftrightarrow 2\,Ti(III) + Co(II). \qquad (1)$$

A longer exposure of cobalt in NaCl-KCl-K_2TiF_6 melt totally shifts the R_1 wave to the anodic region, indicating the presence of only Ti(III) complexes in the melt. The colour after experiment of solidified melt was blue that indicates on the formation of $CoCl_4{}^{2-}$ complexes

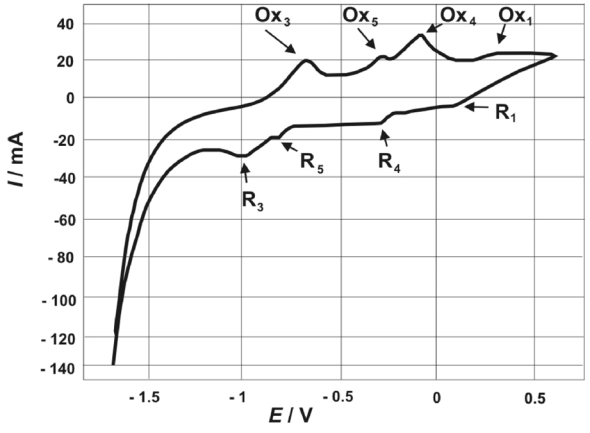

Fig. 4. Cyclic voltammogram at a platinum electrode in NaCl-KCl-K_2TiF_6 melt contacting Co metal. Area: 0.296 cm^2; sweep rate: 1.0 $V\,s^{-1}$; temperature: 1023 K; concentration of $K_2TiF_6 = 9.62 \cdot 10^{-5}$ $mol\,cm^{-3}$; quasi-reference electrode: glassy-carbon.

in the melt, because complexes of Ti(III) are colourless.

Peak R_4 corresponds to cobalt ions discharge to the metal $Co(II) + 2e^- \rightarrow Co$ with its dissolution characterized by peak Ox_4 and cobalt formation at this wave potential was confirmed by potentiostatic electrolysis and XRD analysis of the product obtained.

It was found that the peak discharge current for Co(II) to metal is directly proportional to the square root of the polarization rate, while the peak potential does not depend on the polarization rate, at least up to 0.3 $V\,s^{-1}$. The peak current of the electroreduction process depends linearly on the $CoCl_2$ concentration and peak potential shifted to the positive region with increasing of $CoCl_2$ content. According to the theory of linear sweep voltammetry [7], up to a polarization rate of 0.3 $V\,s^{-1}$, the electrode process is controlled by the rate of mass transfer.

The voltammetric data make possible the calculation of the equilibrium constant of reaction (1) by using the equation [8, 9]

$$\log K^* = \frac{2F}{2.303RT}(E^*_{\mathrm{Ti(IV)/Ti(III)}} - E^*_{\mathrm{Co(II)/Co}}), \quad (2)$$

where $E^*_{\mathrm{Ti(IV)/Ti(III)}}$ and $E^*_{\mathrm{Co(II)/Co}}$ are formal standard potentials.

Kuznetsov et al. [8], have shown that the formal standard potential for a reversible process with the formation of a soluble form in the melt can be calculated from

$$E^*_{\mathrm{Ti(IV)/Ti(III)}} = E_p^{\mathrm{Ti(IV)/Ti(III)}} + 1.11\frac{RT}{F} + \frac{RT}{F}\ln\left(\frac{D_{\mathrm{Ti(IV)}}}{D_{\mathrm{Ti(III)}}}\right)^{1/2}, \quad (3)$$

where $D_{\mathrm{Ti(IV)}}$ and $D_{\mathrm{Ti(III)}}$ are diffusion coefficients of the oxidized and reduced forms.

Assuming $\left(\frac{D_{\mathrm{Ti(IV)}}}{D_{\mathrm{Ti(III)}}}\right)^{1/2} \cong 1$, (3) becomes

$$E^*_{\mathrm{Ti(IV)/Ti(III)}} = E_p^{\mathrm{Ti(IV)/Ti(III)}} + 1.11\frac{RT}{F}. \quad (4)$$

In the case when the process is reversible with an insoluble product, for instance, formation of metal, the formal standard potential can be calculated [10] from the linear voltammetry data by

$$E^*_{\mathrm{Co(II)/Co}} = E_p^{\mathrm{Co}} - \frac{RT}{2F}\ln N_{\mathrm{Co}} + 0.854\frac{RT}{2F}, \quad (5)$$

where N_{Co} is the metal ion concentration in the melt as molar fraction, created by addition of $CoCl_2$ to the NaCl-KCl-K_2TiF_6 melt.

Using (2), we calculated for reaction (1) the logarithm of the equilibrium constant as equal to 3.30 at 1023 K. Thus, reaction (1) was entirely shifted to the right hand side. Indeed, the concentration of cobalt (II) calculated from reaction (1) and determined by chemical analysis were essentially the same.

To gain insight into the processes occurring at potentials corresponding to wave R_5, we conducted potentiostatic electrolysis at the above wave potentials and galvanostatic electrolysis at a current density higher than the limiting diffusion current density for cobalt ion discharge. The result of these electrolyses is the formation of an intermetallic compound Co_3Ti (according to XRD). Thus, the R_5 and Ox_5 peaks correspond to the formation of the intermetallic compound Co_3Ti and its dissolution.

The scheme of cobalt electodeposition from NaCl-KCl-K_2TiF_6 melt in contact with cobalt metal (Fig. 5) shows that cobalt metal can be produced at cathodic current densities lower than the limiting diffusion current density of process R_4.

The limiting diffusion current density of cobalt ion discharge depends on the cobalt concentration in the melt, temperature and hydrodynamic conditions in the electrolyser. At cathodic current densities higher than

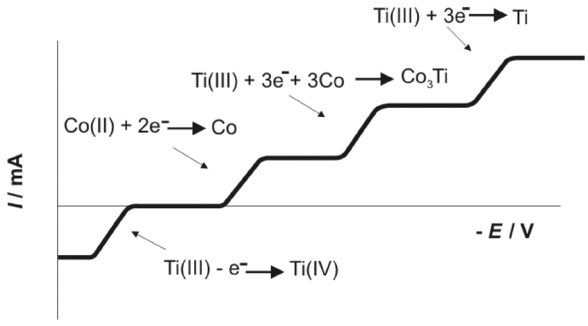

Fig. 5. Scheme of electrodeposition of cobalt and intermetallic compound Co_3Ti from NaCl-KCl-K_2TiF_6 melt in contact with Co metal.

the limiting diffusion current density of cobalt ions discharge the intermetallic compound formed at the cathode is Co_3Ti (Fig. 5).

The limiting current density of cobalt ions discharge ($i_{\text{lim.}}$ in NaCl-KCl-K_2TiF_6 (20 wt%)-$CoCl_2$ melt was determined by steady-state voltammetry ($v = 5 \cdot 10^{-3}$ V s^{-1}) within a $CoCl_2$ concentration range 0.5 – 5.0 wt%. At constant temperature, $i_{\text{lim.}}$ can be calculated using the equation of steady-state voltammetry [11]

$$i_{\text{lim.}} = k \cdot C_{\text{Co}(II)}, \tag{6}$$

where k is the constant for limiting current density (A cm^{-2} wt%$^{-1}$) and $C_{\text{Co(II)}}$ is the concentration of cobalt ions in the melt.

The dependence of constant for limiting current density on temperature is given by Galus [7] as

$$k = A \cdot 10^{-B/T}, \tag{7}$$

where A and B are constants.

From (6) and (7), the limiting current density becomes

$$i_{\text{lim.}} = A \cdot 10^{-B/T} \cdot C_{\text{Co(II)}} \tag{8}$$

and is satisfactorily fitted (correlation coefficient R^2 is equal to 0.984) by the empirical dependence

$$i_{\text{lim.}} = 13.5 \cdot 10^{-2064/T} \cdot C_{\text{Co(II)}}. \tag{9}$$

Equation (9) thus enables the limiting diffusion current density to be calculated for cobalt electrolysis with electrolytes of this composition as function of temperature and cobalt concentration in the electrolyte.

Table 1. Formal standard potentials $E^*_{\text{Me}^{n+}/\text{Me}}$ in NaCl-KCl melt [14] relative to a chlorine reference electrode and parameters K; arrows denote how the difference between the formal standard potential of the metal and $E^*_{\text{Co(II)/Co}}$ varies with increasing basicity of the melt.

Me^{n+} / Me	E^* / V	K	Variation of potential difference
Electronegative impurities			
Mg(II)/Mg	−2.67	0.90	↓
Mn(II)/Mn	−2.02	0.78	↓
Al(III)/Al	−1.97	1.81	↑
Ti(II)/Ti	−1.90	0.76	↓
Si(IV)/Si	−1.74	3.25	↑
Zn(II)/Zn	−1.69	0.88	↓
V(II)/V	−1.63	0.82	↓
Cr(II)/Cr	−1.59	0.89	↓
Fe(II)/Fe	−1.34	1.07	↑
Pb(II)/Pb	−1.22	0.55	↓
Sn(II)/Sn	−1.20	0.64	↓
Metal being refined			
Co(II)/Co	−1.16	1	↔
Electropositive impurities			
Cu(I)/Cu	−1.13	0.42	↓
Ni(II)/Ni	−0.97	0.94	↓
Sb(III)/Sb	−0.95	1.28	↑
As(III)/As	−0.93	1.68	↑
Bi(III)/Bi	−0.86	0.95	↓
Ag(I)/Ag	−0.84	0.28	↓
Mo(III)/Mo	−0.79	1.41	↑

3.2. Cobalt Electrorefining in NaCl-KCl-K_2TiF_6 (20 wt%) Melt

The main challenge in electrorefining is separation of impurities having formal standard potentials close to that of the metal being refined. The formal standard potentials of a number of metals and cobalt in NaCl-KCl melt at 1000 K are presented in Table 1. In our case the NaCl-KCl melt contained 20 wt% K_2TiF_6, and may contain free fluoride anions [12] (increasing the melt basicity). Kuznetsov has shown [13] that the coefficients of metal and impurity separation on transition from the chloride melt to electrolytes with greater basicity can be predicted by using the parameter $K = \frac{Z^{n+}_{\text{Me}}}{r^{n+}_{\text{Me}}} / \frac{Z^{m+}_{r}}{r_r}$, i. e. the ratio of ionic potentials of impurity metals to the ionic potential of the metal refined. Table 1 lists the parameter K values and also shows whether the formal standard potentials of impurities approach or decrease from that of cobalt when the melt basicity is increased.

Table 1 shows that the formal standard potentials of impurities [14] approach that of the metal being refined for electropositive impurities at $K > 1$ and, consequently, the separation coefficients decrease, since the shift of potentials to the cathodic region is stronger for

Table 2. Content of impurities in cobalt before and after electrorefining in NaCl-KCl-K_2TiF_6 (20 wt%) melt. Temperature 1023 K, current density 0.4 A cm^{-2}.

Impurity	Impurity content, ppm		Purification coefficient
	Initial cobalt	After electrorefining	
Mn	1000	< 10	> 100
Mg	30	< 10	> 3
Si	1000	10	100
Fe	3000	100	30
Al	1000	10	100
Mo	10	< 3	>3
Ti	100	300 – 1000	0.1 – 0.3
Cu	300	< 1	> 300
Ni	5000	100	50
Ca	300	< 30	> 10
Ba	300	< 10	> 30
Zn	100	< 30	> 3
C	400	≤ 10	≥ 40
N_2	200	< 3	> 67
O_2	2000	10	200
H_2	500	< 10	> 50

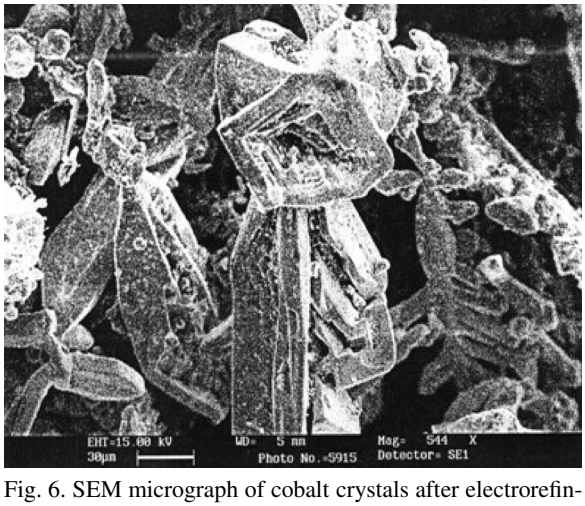

Fig. 6. SEM micrograph of cobalt crystals after electrorefining in NaCl-KCl-K_2TiF_6 (20 wt%). Initial cathodic current density: 0.3 A cm^{-2}; temperature: 973 K.

impurities, compared with that for the metal being refined. For electronegative impurities, at $K > 1$, their shift to the cathodic region also exceeds that for the metal being refined, but in this case the separation coefficients increase. The parameter K does not take into account all contributing factors, one such the alloying of impurities with the metal being refined to give intermetallic compounds, but it is simple and may be useful for the prediction of separation coefficients.

The effectiveness of electrochemical separation of metals during their deposition at the cathode is commonly characterised by the value of separation coefficient θ, which is the quotient of the ratios of the mole fraction of the separated metals M_1 and M_2 in the electrolyte (c_1, c_2) and in the alloy ($x_1^{\text{m.ph.}}$, $x_2^{\text{m.ph.}}$) [15]

$$\theta = \frac{c_1 x_2^{\text{m.ph.}}}{c_2 x_1^{\text{m.ph.}}}. \tag{10}$$

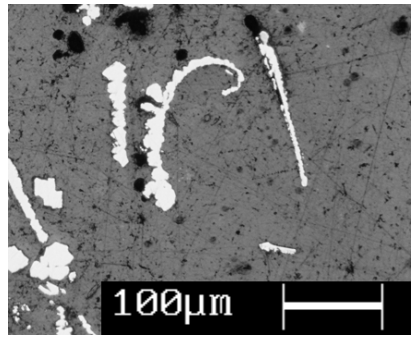

Fig. 7. Crystal of cobalt after bending.

The equation for calculating the separation coefficients (θ) of two metals has the following form [15, 16]:

$$\ln \theta^* = \frac{(n_1 - n_2)FE + n_2 FE_2^* - n_1 FE_1^*}{RT} + \ln \frac{\gamma_1^{\text{m.ph.}}}{\gamma_2^{\text{m.ph.}}}, \tag{11}$$

where E is the alloy potential; E_1^*, E_2^* are formal standard potentials of the metals separated; n_1, n_2 are the oxidation states of the ions; $\gamma_1^{\text{m.ph.}}$, $\gamma_2^{\text{m.ph.}}$ are the activity coefficients of components in the metal phase.

If there is no interaction in the metal phase and $n_1 = n_2 = n$, then the separation coefficient is only determined by the difference between the standard formal metals potentials [15, 16]

$$\ln \theta^* = \frac{nF}{RT}(E_2^* - E_1^*). \tag{12}$$

Equation (12) may only be helpful for calculating the separation coefficient for the pair Co-Ni, which, at 1000 K, is 82.3. Other metals, with an oxidation state +II (Table 1), form intermetallic compounds with cobalt, which makes equation (12) inapplicable.

Table 2 presents the contents of metal and interstitial impurities in cobalt before and after electrorefining in NaCl-KCl-K_2TiF_6 (20 wt%) melt and purification coefficients (the ratio of impurity concentration in cobalt before and after electrorefining). It also makes clear that the concentration of the electronegative impurities Mg, Mn, Al, and Si in cobalt after electrorefining are low, whereas that of Ti increased, apparently

due to the presence of K_2TiF_6 in the electrolyte. Unfortunately, Table 2 cannot contain data on the significant cobalt impurities As and Sb due to the complexity of analysis involved. The fairly high Ti and Ni content in cobalt are not crucial since the cobalt is intended for nickel-titanium alloy production. Figure 6 shows a micrograph of cobalt crystals after electrorefining.

Electrorefining allows the elimination of most of the interstitial impurities, with the result that the remaining impurity levels below 10 ppm impart high ductility to cobalt. Figure 7 shows that the highly pliant cobalt crystal remains unbroken upon bending. We note that using NaCl-KCl-$CoCl_2$ melt as electrolyte does not provide the same degree of cobalt purification from oxygen as that obtained with K_2TiF_6, since it accepts oxygen anions [17].

4. Conclusion

The electrorefining of cobalt in NaCl-KCl-K_2TiF_6 (20 wt%) melt was carried out in hermetic electrolyser under argon atmosphere. It was shown that the concentration of electronegative impurities Mg, Mn, Al, and Si in cobalt after electrorefining was low (10 ppm). At the same time the titanium concentration in cobalt increased, apparently due to the presence of K_2TiF_6 in the electrolyte. The purification coefficients for metallic and interstitial impurities were determined. The purification coefficients for Fe, Ni, and Cu having formal standard potentials close to cobalt were $10-30$, 50 and > 300, respectively. The concentration of each interstitial impurity in refined cobalt was less than 10 ppm that imparts high ductility to cobalt and highly pliant cobalt crystals remain unbroken upon bending.

[1] M. Sorlie and H. Oye, Metallurgy **40**, 67 (1982).
[2] N. Adhoum, J. Bouteillon, D. Dumas, and J. C. Poignet, Electrochim. Acta **51**, 5402 (2006).
[3] V. N. Nekrasov, N. M. Barbin, and L. E. Ivanovskiy, Rasplavy Melts **3**, 51 (1989).
[4] F. Lantelme, K. Kuroda, and A. Barhoun, Electrochim. Acta **44**, 421 (1988).
[5] T. B. Massalski (Ed.), Binary Alloy Phase Diagrams, ASM International, Materials Park, OH 1990.
[6] R. P. Elliot, Constitution of Binary Alloys, McGraw-Hill, New York 1965.
[7] Z. Galus, Fundamentals of Electrochemical Analysis, Ellis Harwood, London 1994.
[8] S. A. Kuznetsov, E. G. Polyakov, and P. T. Stangrit, Dokl. Akad. Nauk. USSR **273**, 653 (1983).
[9] S. A. Kuznetsov, Russ. J. Electrochem. **35**, 1318 (1999).
[10] P. Delahay, New Instrumental Methods in Electrochemistry Theory, Instrumentation and Application to Analytical and Physical Chemistry, Interscience, New York 1954.
[11] Y. Geirovskiy and Y. Kuta, Principles of Polarography, Academic Press, NewYork 1966.
[12] S. A. Kuznetsov, A. L. Glagolevskaya, V. V. Grinevitch, and P. T. Stangrit, Russ. J. Electrochem. **28**, 1344 (1992).
[13] S. A. Kuznetsov, Russ. J. Appl. Chem. **72**, 1804 (1999).
[14] A. N. Baraboshkin, Electrocrystallization of Metals from Molten Salts, Nauka, Moscow 1976.
[15] V. A. Lebedev, Selectivity of Liquid-Metal Electrodes in Halide Melts, Metallurgy, Chelyabinsk 1993.
[16] S. A. Kuznetsov, H. Hayashi, K. Minato, and M. Gaune-Escard, Electrochim. Acta **51**, 2463 (2006).
[17] S. A. Kuznetsov, E. G. Polyakov, and P. T. Stangrit, Russ. J. Appl. Chem. **56**, 427 (1983).